Inorganic Chemistry

Article

pubs.acs.org/IC

Extension of Novel Lanthanide Luminescent Mesoporous Nanostructures to Detect Fluoride

Zhan Zhou,[‡] Yuhui Zheng,[‡] and Qianming Wang*[,†,‡,§]

[†]Key Laboratory of Theoretical Chemistry of Environment, Ministry of Education, School of Chemistry and Environment, South China Normal University, Guangzhou 510006, P. R. China

[‡]School of Chemistry and Environment, South China Normal University, Guangzhou 510006, P. R. China

[§]Key Laboratory of the materials for Energy Conversion and Storage, Guangzhou 510006, P. R. China

Supporting Information

ABSTRACT: A novel polydentate type ligand derived from N^2,N^6-bis(4,4-diethoxy-9-oxo-3-oxa-8,10-diaza-4-siladodecan-12-yl)pyridine-2,6-dicarboxamide (**L**) has been designed, and it played essential roles in the assembly of new organic–inorganic functional materials. First, its multiple amide groups would coordinate to lanthanide ions firmly and transfer the absorbed energy to both Eu(III) and Tb(III) simultaneously. Second, the hydrogen-bond donor units showed strong affinity to guest anion (F^-). Third, the two silylated arms could induce the formation of sol–gel derived siloxane hybrid materials. Following this idea, two lanthanide luminescent amorphous particles (**ASNs-Eu** and **ASNs-Tb**) have been prepared for the recognition of fluoride ions. Further modification of the synthesis method and transformation to mesoporous network (**MSNs-Eu** and **MSNs-Tb**) led to much enhanced thermostabilities, larger specific surface area (from 78.5 to 515 $m^2\ g^{-1}$ for Eu(III); 89.6 to 487 $m^2\ g^{-1}$ for Tb(III)), and lower detection limits (2.5×10^{-8} M for **MSNs-Eu** and 3.4×10^{-8} M for **MSNs-Tb**) for the fluoride ion.

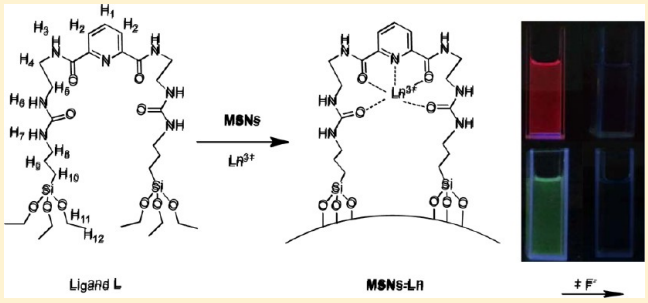

INTRODUCTION

The development and preparation of fluorescent sensors that can selectively recognize and signal the presence of anions have received current attention since they play important roles in many biological and chemical processes.[1−5] Among them, fluoride is considered as a serious health hazard in the environment because it may lead to bone disease or be widely used in organic synthesis.[6,7] Therefore, taking into account the importance of fluoride, many efforts have been made to design simple and low cost sensors.

Recently, lanthanide complexes have been extensively studied owing to their sharp and intense emission peaks, high-quantum efficiencies, and large Stokes shifts which can be applied in the field of optical sensors.[8−15] However, their poor thermal stabilities and low-mechanical strength critically restrict their uses for practical applications. In order to solve these problems, some lanthanide complexes have been incorporated into solid matrices, such as polymers, silica, and soft materials. Their optical and thermal stabilities will be enhanced.[16−20] In the previous work, several solid-based probes activated by lanthanide ions for the detection of fluoride ions have been fabricated in our group.[21,22] Compared with conventional bulk materials, mesoporous nanospheres with large surface area, pore volume, hydrophilicity, and easy recyclability would allow them to be favorably used as heterogeneous optical sensors for highly sensitive detection of specific analytes. In this paper, we designed and synthesized a novel mesoporous system for the fluorogenic detection of anions. The precursor N^2,N^6-bis(4,4-diethoxy-9-oxo-3-oxa-8,10-diaza-4-siladodecan-12-yl) pyridine-2,6-dicarboxamide (**L**), which contains a multiple urea linkage that can be used as a fluoride ion receptor, was prepared by a simple process (for details, see the Experimental Section). This ligand was proved to be an efficient sensitizer for both red and green luminescence of Eu^{3+} and Tb^{3+} ions due to the suitable energy match and intramolecular energy transfer mechanism. It also can be hydrolyzed to assemble on the surface and pores of the mesoporous silica nanoparticles (**MSNs**) by covalent bonds. The emissions of the two target nanoprobes (**MSNs-Eu** and **MSNs-Tb**) were quenched only by F^-. According to the titration of ^1H NMR spectroscopy, we demonstrated that the strong hydrogen bonding interaction between F^- and **L** played an important role in the quenching process.

EXPERIMENTAL SECTION

Materials. Eu_2O_3 (99.9%) and Tb_4O_7 (99.9%) were purchased from Shanghai Yuelong. Europium hydrochlorate was prepared by dissolving Eu_2O_3 in concentrated hydrochloric acid. Terbium nitrate was obtained by dissolving Tb_4O_7 in concentrated nitric acid. Triton X-100, tetraethyl orthosilicate (TEOS, A.R.), cetyltrimethylammonium bromide (CTAB, A.R.), 3-(triethoxysilyl)propyl isocyanate (TEPIC, 96%), pyridine-2,6-dicarboxylic acid (99%), and 1,4-diaminobutane (98%) were purchased from J&K Scientific. All anions (F^-, Cl^-, Br^-, I^-, and HSO_4^-) as tetrabutylammonium (TBA) salts were purchased from Aldrich. All the other reagents were purchased from Guangzhou Chemical Reagent Factory and used without

Received: October 5, 2013
Published: January 10, 2014

   dx.doi.org/10.1021/ic402524z | Inorg. Chem. 2014, 53, 1530−1536

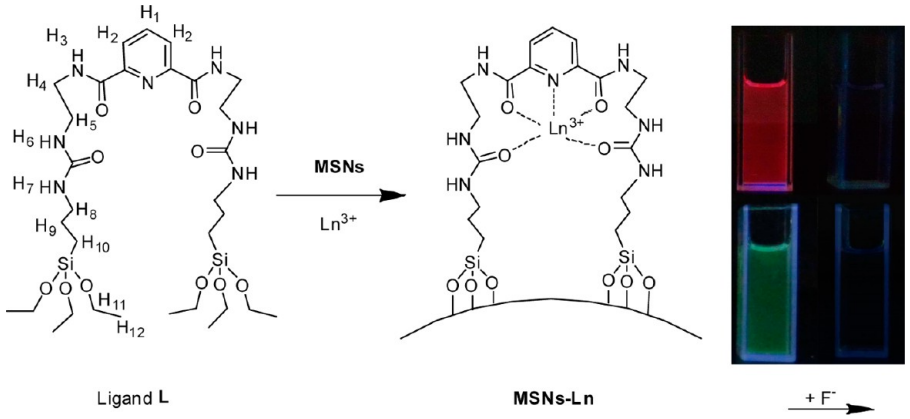

Figure 1. Schematic representation of **MSNs-Eu** and **MSNs-Tb**. Photo: **MSNs-Eu** (top) and **MSNs-Tb** (bottom) in DMSO excited by UV light at 254 and 365 nm with (right) and without (left) fluoride (10^{-5} M).

further purification. N^2,N^6-bis(2-aminoethyl)pyridine-2,6-dicarboxamide was synthesized according to the literature.[23]

Synthesis of Precursor L. N^2,N^6-bis(2-aminoethyl)-pyridine-2,6-dicarboxamide (502 mg, 2 mmol) was dissolved in 25 mL of anhydrous tetrahydrofuran under a steady flow of nitrogen, and TEPIC (1.112 g, 4.5 mmol) was added with magnetic stirring. The mixture was refluxed under nitrogen for 6 h, and the termination of the reaction was monitored by thin layer chromatography. Solvent was removed quickly under reduced pressure to give the crude product. A silica gel column was used to purify the initial product. The crude product was purified on silica gel (petroleum ether/ethyl acetate 20:1→10:1→5:1, v/v) to give the compound N^2,N^6-bis(4,4-diethoxy-9-oxo-3-oxa-8,10-diaza-4-siladodecan-12-yl)pyridine-2,6-dicarboxamide (**L**, yield: 80%) as a white, slightly hygroscopic solid. ^{1}H NMR (400 MHz, $CDCl_3$, ppm): 9.45 (bs, 2H, H_3), 8.26 (d, J = 8.0 Hz, 2H, H_2), 8.07 (t, J = 8.0 Hz, 1H, H_1), 5.74 (bs, 2H, H_6), 5.44 (bs, 2H, H_7), 3.78 (q, J = 13.6 Hz, 12H, H_{11}), 3.58 (t, J = 7.4 Hz, 4H, H_5), 3.50 (t, J = 7.4 Hz, 4H, H_4), 3.11 (t, J = 7.6 Hz, 4H, H_8), 1.58 (m, 4H, H_9), 1.18 (t, J = 7.2 Hz, 18H, H_{12}), 0.58 (t, J = 7.6 Hz, 4H, H_{10}). MS found: m/z 768.7 [M + Na]. Anal. Calcd for [$C_{31}H_{59}N_7O_{10}Si_2$]: C, 49.91; H, 7.97; N, 13.14; O, 21.45; Si, 7.53. Found: C, 49.87; H, 8.05; N, 13.21; O, 21.48; Si, 7.50.

Synthesis of EuL/TbL Complex. To prepare the terbium/europium complex, **L** (0.373 g, 0.5 mmol) was dissolved in 10 mL of ethanol in a 50-mL round-bottom flask. One equivalent of $EuCl_3$/$Tb(NO_3)_3$ (10 mL of a 0.05 M solution, 0.5 mmol) and ammonia (1 mL) were added with magnetic stirring. The mixture was refluxed for 3 h at 90 °C. The crude product was washed with ethanol and water and then dried in vacuo overnight. The resulting precipitate was collected to give the desired Eu**L**/Tb**L** as a white powder.

Fabrication of Amorphous Silica Nanospheres (ASNs) and the Hybrid Material (ASNs-Eu/ASNs-Tb). Amorphous silica nanoparticles were synthesized using the reverse microemulsion method.[24] Briefly, 17.7 g of Triton X-100, 16 mL of n-hexanol, and 75 mL of cyclohexane were mixed in a 250-mL glass flask with forceful magnetic stirring, and 4 mL of deionized H_2O was added. After the addition of 1 mL of TEOS, the solution was stirred for 30 min. To initiate silica polymerization, 0.65 mL of NH_4OH was added. This polymerization was allowed to proceed for 18 h. The particles were centrifuged, sonicated, and vortexed three times with anhydrous ethanol, followed by washing twice with deionized water. The resulting precipitate was dried in vacuo to obtain amorphous silica nanospheres (**ASNs**). To an **ASNs** (200 mg) ethanol suspension, 1 mL of **L** ethanol solution (0.5 M) and 500 μL of aqueous ammonia (30%) were added, and the suspension was stirred for 3 h. Then, $EuCl_3$/$Tb(NO_3)_3$ solution (1 mL, 0.5 M) was added. After 12 h, the precipitate was centrifuged and redispersed in ethanol and water at least three times to remove excess unreacted **L** and lanthanide ions. The precipitate was dried in vacuo to obtain the target materials (**ASNs-Eu**/**ASNs-Tb**).

Fabrication of Mesoporous Silica Nanospheres (MSNs) and the Hybrid Material (MSNs-Eu/MSNs-Tb). **MSNs** were synthesized using the hydrothermal method reported in the literature.[25] Briefly, the above prepared amorphous silica nanospheres (**ASNs**) were dispersed into water by sonication. Then 1 mL of the dispersion (containing 0.03 g silica) was mixed with 0.1 g of cetyltrimethylammonium bromide (CTAB), 0.6 g of urea, and 30 mL of water in an autoclave. The mixture was sonicated to make a uniform dispersion. Finally the autoclave was sealed and hydrothermally heated at 180 °C for 24 h. Then, the autoclave was naturally cooled in the oven. After hydrothermal treatment, the precipitate was centrifuged and calcined at 550 °C for 5 h to remove the surfactant moiety. The residue was the mesoporous silica nanospheres (**MSNs**). In a **MSN** (200 mg) ethanol suspension, 1 mL of **L** ethanol solution (0.5 M) and 500 μL of aqueous ammonia (30%) were added, and the suspension was stirred for 3 h. Then, $EuCl_3$/$Tb(NO_3)_3$ solution (1 mL, 0.5 M) was added. After 12 h, the precipitate was centrifuged and redispersed in ethanol and water at least three times to remove excess unreacted **L** and lanthanide ions. The precipitate was dried in vacuo to give the target materials (**MSNs-Eu**/**MSNs-Tb**).

Characterizations. ^{1}H NMR spectra were recorded at 293 K using a Varian 400 (400 MHz) with tetramethylsilane, $Si(CH_3)_4$, as an internal standard; all chemical shifts were reported in the standard notation of parts per million. Fluorescence and excitation spectra were measured using an Edinburgh FLS920 spectrometer (UK), equipped with a 50 W mercury lamp source. FT-IR spectra were measured using a Shimadzu Prestige-21. Transmission electron microscopy (TEM) was carried out by using a JEOL JEM-2100HR transmission electron microscope. Scanning electron microscopy (SEM) was measured using a Zeiss Ultra 55 scanning electron microscope. The adsorption desorption isotherms of

dx.doi.org/10.1021/ic402524z | Inorg. Chem. 2014, 53, 1530−1536

nitrogen were measured at 77 K using the ASAP2020 M system. Thermogravimetric analysis (TGA) was carried out on a STA409PC system under air at a rate of 10 °C/min. The X-ray diffraction (XRD) measurements were carried out on powdered samples via a BRUKER D8 diffractometer (40 mA/40 kV), using monochromated Cu Kα_1 radiation (λ = 1.54 Å). Mass spectra (MS) were obtained on a Thermo Finnigan LCQ Deca XP Max. Elemental analyses were conducted on a ThermoElectrons FlashEA 1112. Dynamic light scattering measurements were performed on a Malvern Mastersizer-2000.

RESULTS AND DISCUSSION

The synthesis process of **MSNs-Ln** is shown in Figure 1. Typically, the as-prepared amorphous silica nanoparticles (**ASNs**) were treated by hydrothermal procedure with CTAB as a surfactant, to result in the formation of the mesoporous silica nanospheres (**MSNs**). Subsequently, the synthetic precursor **L** was covalently grafted onto the interior surface of mesopores and chelated with lanthanide ions (**MSNs-Eu** and **MSNs-Tb**). Moreover, it is quite favorable that efficient energy transfer can be realized in Eu^{3+} and Tb^{3+} based on the same silylated ligand in view of analytical and structural probes.

The precursor **L**, **MSNs-Eu**, and **ASNs-Eu** were characterized by FT-IR spectroscopy (Figure 2). From the figure of

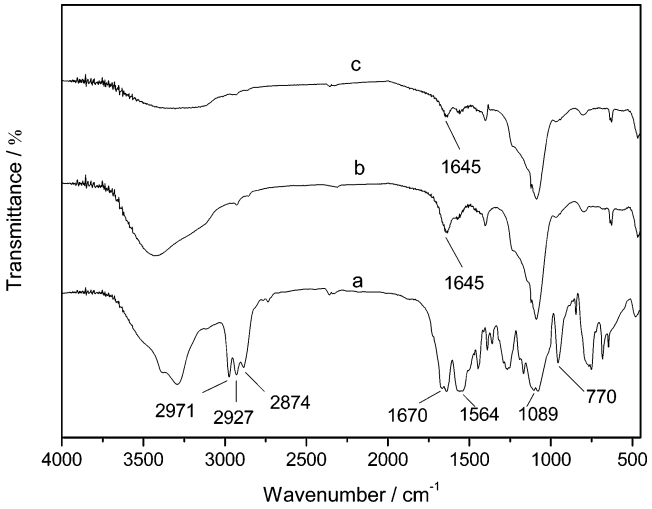

Figure 2. IR spectra of the ligand **L** (a), **MSNs-Eu** (b), and **ASNs-Eu** (c).

the precursor (Figure 2a), three adjacent peaks at 2971, 2927, and 2874 cm^{-1} were detected to correspond to C−H stretching vibrations of methyl and methylene groups. The sharp bands located at 1670 and 1564 cm^{-1} ascribed to the urea NH−CO−NH groups indicated that the reaction between N^2,N^6-bis(2-aminoethyl)pyridine-2,6-dicarboxamide and TEPIC was successful. Moreover, the characteristic bands of the Si−O and N−H bending mode at 1089 and 770 cm^{-1} were also observed. As shown in Figure 2b, the ν(C═O) vibration was shifted to lower frequency (from 1670 to 1645 cm^{-1}) compared with that of **L**, which can indicate the complexation of the europium ions with the oxygen atom of the carbonyl group.[26,27] Similar results were observed in the FT-IR spectrum of **ASNs-Eu** (Figure 2c). At the same time, we also studied the **MSNs-Tb** and **ASNs-Tb** (Figure S1) by infrared spectroscopy, and these spectra were similar with those of **MSNs-Eu** and **ASNs-Eu**, verifying the same coordination mode of these hybrid materials with different lanthanide ions.

The photoluminescence and anion-binding abilities of **MSNs-Eu** were investigated using fluorescence spectroscopy in DMSO at concentrations as low as 1 mg/L. The overall luminescence changes of **MSNs-Eu** upon titration of F^- are shown in Figure 3. When the emission wavelength was

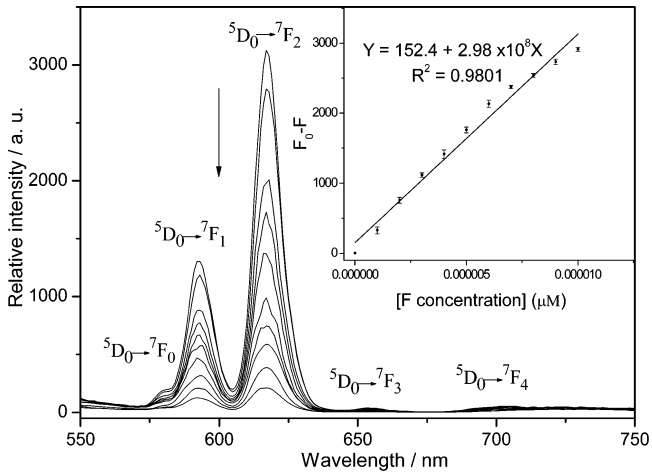

Figure 3. Emission spectra of **MSNs-Eu** (1 mg/L, λ_{ex} = 280 nm) upon the addition of 10^{-6} to 10^{-5} M F^- in DMSO. Inset: Relative intensity of **MSNs-Eu** at 616 nm with the concentration over a F^- concentration range from 10^{-6} to 10^{-5} M.

monitored at 616 nm, the excitation spectrum shows a broad band covering from 250 to 310 nm with the maximum at 280 nm (Figure S2). A series of narrow-width emission bands (λ_{ex} = 280 nm) with maxima at 580, 592, 616, 654, and 704 nm were recorded, and they were attributed to the $^5D_0 \rightarrow {}^7F_J$ (J = 0, 1, 2, 3, and 4) transitions of Eu^{3+} ions. The emission intensities of **MSNs-Eu** significantly declined and was almost completely quenched with increasing fluoride anion amounts. This distinguished quenching effect can even be detected by the naked eye under the excitation of the UV light (Figure 1, inset photo). The plot of $F_0 - F$ (difference value between F_0 and F) versus the fluoride concentration (from 10^{-6} to 10^{-5} mol/L) follows a simple linear function $Y = 152.4 + (2.98 \times 10^8)X$ (R^2 = 0.9801) by the least-squares fitting method (Figure 3, inset). F_0 or F is the luminescence intensity of **MSNs-Eu** at 616 nm without or with the addition of fluoride ions. Parallel experiments were carried out 10 times, and the standard error bars on the measured data were shown in Figure 3 (inset). The limit of detection (LOD) for F^- was 2.5×10^{-8} M, which was measured by LOD = 3SD/slope (the above linear function). SD is the standard deviation of the blank sample (obtained by 10 consecutive scans of the blank sample).

We also studied the anion-binding abilities of **ASNs-Eu** under the same conditions (Figure S3). The emission intensity of **ASNs-Eu** was 10 times less than that of **MSNs-Eu** due to the immobilization of smaller amounts of receptor **L** on silica particles via covalent bonding. It has been found that the calculated LOD of **ASN-Eu** (1×10^{-6} M) was much higher than that of **MSNs-Eu**, proving the extended surface area could induce more sensitive luminescence changes to the same analyte. Anyway, the receptor bearing multiple amide groups has played an important role in the selective sensing of fluoride since both **MSNs-Eu** and **ASN-Eu** were responsive to the

dx.doi.org/10.1021/ic402524z | Inorg. Chem. 2014, 53, 1530−1536

anion. On the other hand, no significant fluorescence changes of **MSNs-Eu** and **ASNs-Eu** were observed upon the addition of 10^{-5} M Cl^-, Br^-, I^-, or HSO_4^- (Figures S3 and S4). Therefore, we considered that **MSNs-Eu** with its large surface area can be used as a luminescent sensor specific for the detection of F^-.

In a similar fashion, we also investigated the sensing abilities of **MSNs-Tb** and **ASNs-Tb**. The emission spectra of **MSNs-Tb** and **ASNs-Tb** (excited at 282 nm) can be interpreted as follows: the $^5D_4 \rightarrow {}^7F_J$ transitions exhibit four main components for J = 6, 5, 4, and 3, respectively. As shown in Figure 4, the

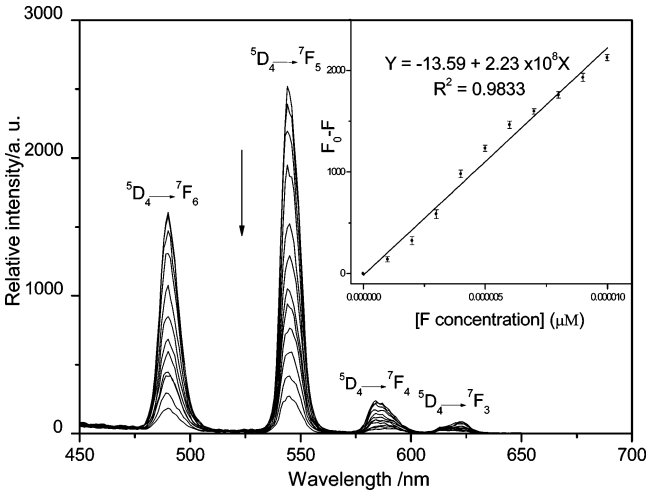

Figure 4. Emission spectra of **MSNs-Tb** (1 mg/L, λ_{ex} = 282 nm) upon the addition of 10^{-6} to 10^{-5} M F^- in DMSO. Inset: Relative intensity of **MSNs-Tb** at 545 nm with the concentration over a F^- concentration range from 10^{-6} to 10^{-5} M.

luminescence of **MSNs-Tb** has reduced with the F^- concentration increase (from 10^{-6} to 10^{-5} M). When plotting $F_0 - F$ ($^5D_4 \rightarrow {}^7F_5$ emission) against the concentration in the range of 10^{-6} to 10^{-5} M, we observed that the calibration region follows the linear equation $Y = -13.59 + (2.23 \times 10^8)X$ by the least-squares fitting method and the correlation coefficient R^2 = 0.9833 (Figure 4, inset). The calculated LOD of **MSNs-Tb** for F^- was 3.4×10^{-8} M. The selectivity of **ASN-Tb** for anions was similar to that of **MSNs-Tb**, whereas its LOD (2.1×10^{-6} M) for fluoride ions was much higher than that of **MSNs-Tb**. The above results were consistent with the sensing abilities of **MSNs-Eu** and **ASNs-Eu**. It is indicated that mesoporous silica with its large surface area is useful as a support material. Moreover, analogous experiments were performed by the titration of 10^{-5} mol/L of Cl^-, Br^-, I^-, or HSO_4^- by fluorescence spectroscopy (Figures S5 ad S6). Almost no changes could be detected in the emission spectra. Consequently, we can draw the conclusion that **MSNs-Tb** may be taken as a chemical sensor specific for the fluoride ion as well as **MSNs-Eu**.

Generally speaking, the NH group is likely to participate in the hydrogen bonding interactions. In the past decade, many references indicated that the NH of urea forms hydrogen bonds with fluoride anions.[28−30] Therefore, the mechanism for the emission changes of the target hybrid materials could be explained as a hydrogen-bonding interaction between F^- and NH of the organic moiety. In detail, the strong fluoride binding changed the coordination conformation and affected the efficiency of energy transfer between ligand and lanthanide ions. To further verify the proposed sensing mechanism, ^{1}H NMR spectroscopy was applied to investigate the nature of the interaction between **L** and anions. Figure 5 shows the ^{1}H NMR

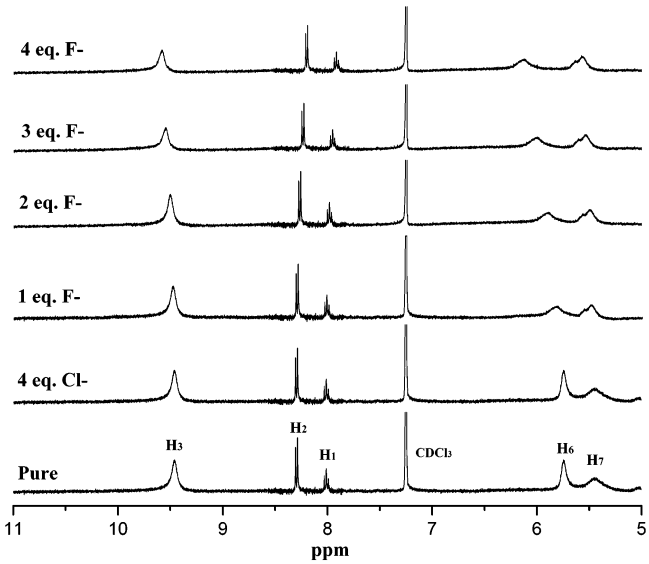

Figure 5. ^{1}H NMR spectra of ligand **L** (bottom) in the presence of 4 equiv. of Cl^- and various equivalents of F^- in DMSO-d_6.

spectral changes of **L** in the absence and presence of chloride and various equivalents of fluoride anions. Obviously, the N−H signals at 9.45, 5.74, and 5.44 ppm, which have been assigned to H_3, H_6, and H_7 (marked in Figure 1), respectively, can be observed in the absence of anions. When we titrated **L** (10 mM) with F^-, all of the N−H signals were shifted downfield. After adding 4 equiv. of F^- (40 mM), these signals were shifted from 9.45, 5.74, and 5.44 to 9.61, 6.15, and 5.61 ppm, respectively. The strong deshielding effects of the corresponding resonances were probably attributed to the strong polarization induced by the H-bonded F^-. Moreover, the signals of the pyridine ring exhibited an upfield shift slightly, being ascribed to electron transfer from anions to the electron-withdrawing pyridine ring. However, 4 equiv. of Cl^- was not able to trigger any changes of hydrogen signals.

In order to avoid the interference of hydrogen-bonding interactions, we studied the sensing capabilities of **MSNS-Eu** for F^- in polar solvents such as water and ethanol. Upon the addition of fluoride (10 μM), the emission intensity of **MSNS-Eu** has reduced slightly (Figure S7). It proved that coordination replacement was also the influencing factor in the recognition process. But we have to say that the luminescence decreased dramatically when the experiment was carried out within DMSO. The results suggested that the hydrogen-bonding formation between F^- and the ligand **L** could not be neglected. In order to further clarify the mechanism, we have investigated the interactions between the pure organic ligand (N^2,N^6-bis(4,4-diethoxy-9-oxo-3-oxa-8,10-diaza-4-siladodecan-12-yl) pyridine-2,6-dicarboxamide, **L**) and the anions. We measured the emission changes of the ligand upon the addition of F^-, Cl^-, Br^-, I^-, and HSO_4^- (Figure S8). Only F^- could quench the singlet excited state of the sensitizing chromophore. It is well accepted that the organic ligand absorbed the ultraviolet energy and migrated it to lanthanide ions. Here, the energy derived from the ligand had been restricted. The energy transfer to lanthanide ions was therefore terminated. Hence, the mutual interactions between the ligand and fluoride would lead

dx.doi.org/10.1021/ic402524z | Inorg. Chem. 2014, 53, 1530−1536

to the luminescence quench in the experiments. If only the factor of coordination replacement played the decisive role, the luminescence quench would have no relationship with the ligand, but the above tests gave different results.

Another point that has to be mentioned is that the luminescent nanoparticles in our system were used as heterogeneous optical sensors for the detection of F^-. In other words, the lanthanide organic complexes were covalently bonded onto the surface of nanosilica (not incorporated into the internal silica structure). Therefore, we considered that F^- anions could have the chance to interact with the urea moieties of the ligand even in the solid state. On the basis of the above experiments and previous references described by Tripier et al.[31,32] and Parker et al.,[33,34] it is estimated that synergistic effects of both coordination replacement and hydrogen bonds would contribute to the emission quenching phenomenon.

We studied the reusabilities of **MSNs-Eu** and **MSNs-Tb** for F^- sensing by dipping−rinsing cycles, and fluorescence spectra were recorded after each step (Figures S9 and S10).[35] After quenching by F^- (10^{-5} M), the sample was isolated by centrifugation and washed with ethanol three times to remove the F^-, then the collected sample was dried in a vacuum. Therefore, the characteristic emission of lanthanide ions was retrieved (emission "on"). It is obvious that both **MSNs-Eu** and **MSNs-Tb** exhibit excellent reusability because very limited losses in their luminescence intensity were observed after 10 repeated cycles.

The thermal stabilities of Eu**L** and **MSNs-Eu** were investigated by thermogravimetric analysis (TGA, Figure 6)

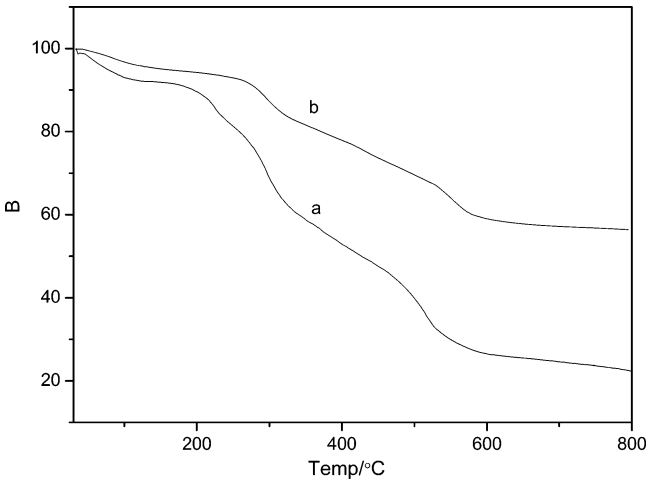

Figure 6. Thermogravimetric analysis traces of Eu**L** (a) and **MSNs-Eu** (b).

experiment. The TG curve of Eu**L** showed two steps of weight loss. The first weight loss of 9% in the range of 25−180 °C is possibly caused by the adsorbed solvent species and coordinated water molecules. An additional 60% weight loss that occurred in the second step (180−560 °C) may be attributed to the collapse of the coordination structures and the decomposition of the organic components. However, **MSNs-Eu** began to lose major weight at 225 and 270 °C, respectively. This fact demonstrated that the formation of organosilicate framework through Si−O covalent bonds and the mesoporous structure effectively restricts the mobility of embedded organic compounds, and the decomposition temperature of **MSNs-Eu** is higher than that of the complex. Similar behaviors were observed in the TG curves of Tb**L** and **MSNs-Tb** (Figure S11).

The powder XRD patterns of the **MSNs**, **MSNs-Eu**, and **MSNs-Tb** were provided in Figure 7. Only one broad Bragg

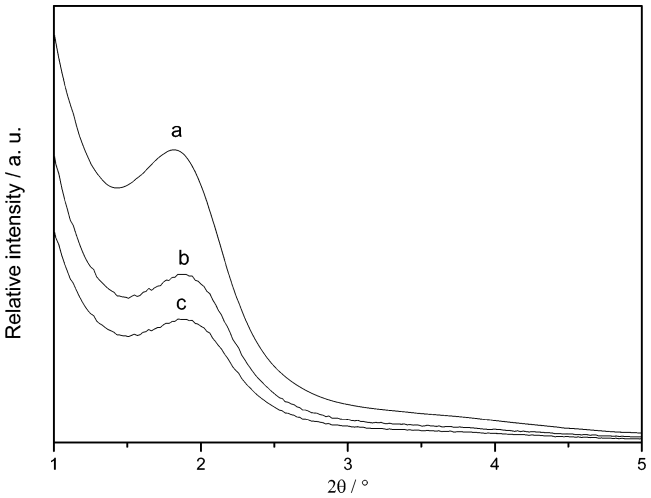

Figure 7. Small-angle XRD patterns of **MSNs** (a), **MSNs-Eu** (b), and **MSNs-Tb** (c).

peak at low angles (2θ = 1.9−2.0) was observed. The results fully indicate that the disordered mesostructures of **MSNs** are maintained after the functionalization of lanthanide complexes. In general, the highly ordered bulk materials (for example SBA-15) possess multiple sharp peaks in the low angle range ($0.6° < 2\theta < 6°$), while our samples only give one broad peak at a low angle. This is because that XRD peaks become broadened or disappear with a decreasing of particle size or disordering of mesostructure. As for the X-ray diffraction of **ASNs-Eu** and **ASNs-Tb** (Figure S12), the absence of long-range order as determined by XRD implied that these nanoparticles are amorphous. It can be seen that all the diffraction curves exhibit similar broad peaks with the angle 2θ centered around 23°, which is characteristic of amorphous silica materials.[36]

Classical nitrogen adsorption−desorption isotherms are used as a macroscopic average measurement for exploring the pore structure of the materials. The corresponding isotherms of **MSNs**, **MSNs-Eu**, and **MSNs-Tb** are displayed in Figure 8. The specific area is calculated by the Brunauer−Emmett−Teller (BET) method, and the pore size is calculated by BJH model. The BET surface areas of **MSNs-Eu** and **MSNs-Tb** are 515 and 487 $m^2\ g^{-1}$, respectively, and the total pore volumes are 0.43 and 0.40 $cm^{-3}\ g^{-1}$, respectively. Compared with pure **MSNs** (BET = 927 $m^2\ g^{-1}$, pore volume = 1.07 $cm^{-3}\ g^{-1}$), the introduction of the lanthanide complexes induced an obvious decrease of the above data, which is consistent with the presence of anchored organic ligands in the pore channels of **MSNs**. We also investigated the N_2 adsorption−desorption isotherms of **ASNs**, **ASNs-Eu**, and **ASNs-Tb** (Figure S13). The BET surface areas are 150.8, 78.5, and 89.6 $m^2\ g^{-1}$, respectively. Compared with the mesoporous backbone, the surface area of amorphous samples was significantly reduced. In addition, the lanthanide (III) complex−functionalized amorphous silica nanoparticles decrease considerably compared to the original **ASNs** sample, which again supports that the organic ligands would firmly bind to the surface of the silica even after washing several times.

dx.doi.org/10.1021/ic402524z | Inorg. Chem. 2014, 53, 1530−1536

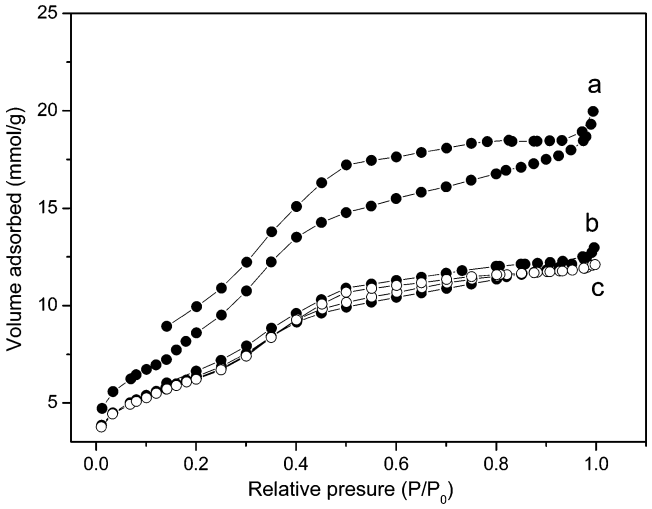

Figure 8. Nitrogen adsorption−desorption curves of **MSNs** (a), **MSNs-Eu** (b), and **MSNs-Tb** (c).

The morphology and size of prepared **MSNs-Eu** and **ASNs-Eu** were investigated by transmission electron microscopy (TEM). The obtained **MSNs-Eu** had uniform spherical structures with an average diameter of 300 ± 10 nm (Figure 9a) by manually measuring over 100 particles. The morphology of **MSNs-Eu** was comparable with that of pure **MSNs** (Figure S14), indicating that the grafted organic structures did not change their microstructures significantly. Particularly, very tiny pores like structures were also clearly identified in the high resolution transmission electron microscopy (HRTEM) image (Figure 9b), which coincided with the XRD analyses (Figure 7). **ASNs-Eu** exhibited a monodispersed spherical morphology with a diameter of approximately 61 nm, and no observable change was seen in morphology after the lanthanide complexes were covalently coated onto the silica host (Figures 9c and S14b). In contrast to **MSNs-Eu**, no mesopores in the HRTEM image (Figure 9d) could be found in the corresponding amorphous silica. Moreover, the similar structures of **MSNs-Eu** and **ASNs-Eu** were also obtained in their SEM images and dynamic light scattering curves (Figure S15 and S16).

CONCLUSIONS

In summary, the ligand **L** with a triethoxysilane moiety could generate a sol−gel reaction in situ within the matrix, and it could efficiently sensitize emissions of both the Eu(III) and Tb(III) ions. Additionally, the hydrogen bonding between anion and precursor **L** resulted in the sensing process in view of NMR analysis. The luminescence detection of the fluoride ion was successfully demonstrated using lanthanide complex modified mesoporous silica nanoprobes (**MSNs-Eu** and **MSNs-Tb**). Compared with amorphous probes (**ASNs-Eu** and **ASNs-Tb**), these nanoprobes possessed remarkable properties, including higher thermostability, larger specific surface area, and lower detection limit specific for the fluoride ion. This work will be the subject of future studies and adapted to other related anions.

ASSOCIATED CONTENT

Supporting Information

IR spectra of **L**, **MSNs-Tb** and **ASNs-Tb**; excitation spectra of **MSNs-Eu**; emission spectra of **ASNs-Eu**, **MSNs-Eu**, **ASNs-Tb**, and **MSNs-Tb**; emission and excitation spectra of **L**; recycled experiments of **MSNs-Eu** and **MSNs-Tb**; thermogravimetric analysis traces of Tb**L**, **ASNs-Tb**, and **MSNs-Tb**; XRD patterns of **ASNs-Eu** and **ASNs-Tb**; nitrogen adsorption−desorption curves of **ASNs**, **ASNs-Eu**, and **ASNs-Tb**; TEM images of **MSNs** and **ASNs**; SEM images of **MSNs-Eu** and **ASNs-Eu**; size distribution graphs of **MSNs**, **MSNs-Eu**, **ASNs**, and **ASNs-Eu**. This material is available free of charge via the Internet at http://pubs.acs.org.

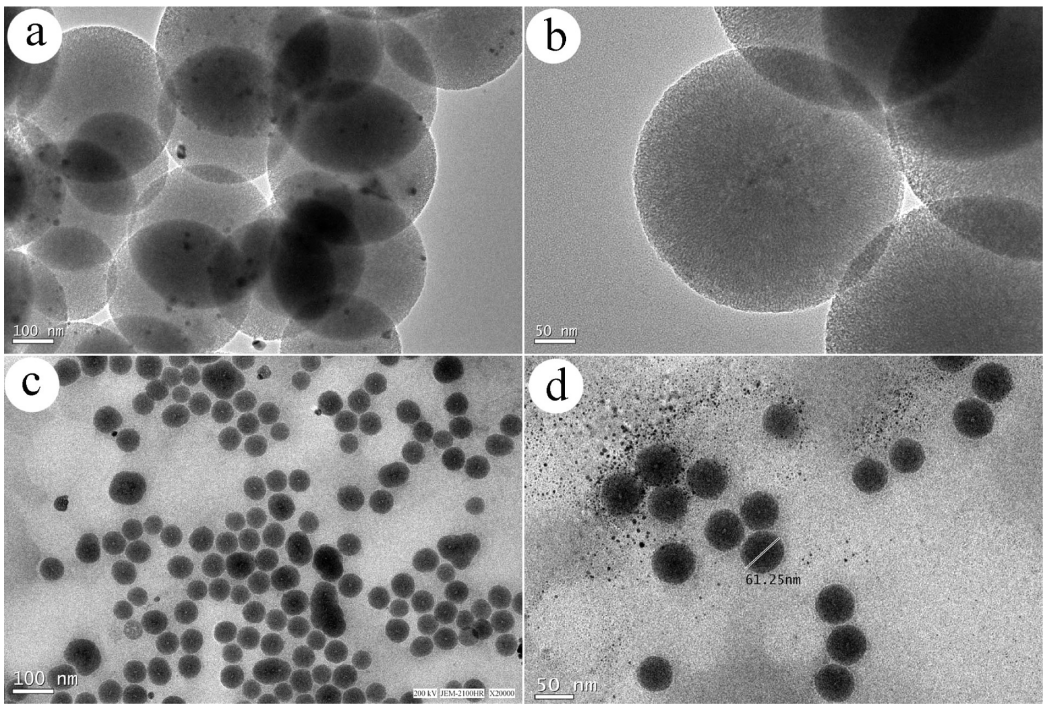

Figure 9. TEM images of **MSNs-Eu** (a, b) and **ASNs-Eu** (c, d).

dx.doi.org/10.1021/ic402524z | Inorg. Chem. 2014, 53, 1530−1536

AUTHOR INFORMATION

Corresponding Author

*Tel.: 86-20-39310258. Fax: 86-20-39310187. E-mail: qmwang@scnu.edu.cn.

Notes

The authors declare no competing financial interest.

ACKNOWLEDGMENTS

Q.W. acknowledges the support from National Natural Science Foundation of China (No. 21371063 and No. 21002035). This study was supported by the Scientific Research Foundation of Graduate School of South China Normal University.

REFERENCES

(1) Santos-Figueroa, L. E.; Moragues, M. E.; Climent, E.; Agostini, A.; Martínez-Máñez, R.; Sancenón, F. *Chem. Soc. Rev.* **2013**, *42*, 3489−3613.

(2) Aldrey, A.; Núñez, C.; García, V.; Bastida, R.; Lodeiro, C.; Macías, A. *Tetrahedron* **2010**, *66*, 9223−9230.

(3) Anzenbacher, J. P.; Jursíková, K.; Sessler, J. L. *J. Am. Chem. Soc.* **2000**, *122*, 9350−9351.

(4) Das, P.; Mandal, A. K.; Kesharwani, M. K.; Suresh, E.; Ganguly, B.; Das, A. *Chem. Commun.* **2011**, *47*, 7398−7400.

(5) Mizukami, S.; Nagano, T.; Urano, Y.; Odani, A.; Kikuchi, K. *J. Am. Chem. Soc.* **2002**, *124*, 3920−3925.

(6) Yeamans, C. B.; Silva, G. W. C.; Cerefice, G. S.; Czerwinski, K. R.; Hartmann, T.; Burrell, A. K.; Sattelberger, A. P. *J. Nucl. Mater.* **2008**, *374*, 75−78.

(7) Villalba1, G.; Ayres, R. U.; Schroder, H. *J. Ind. Ecol.* **2007**, *11*, 85−101.

(8) Eliseeva, S. V.; Bünzli, J.-C. G. *Chem. Soc. Rev.* **2010**, *39*, 189−227.

(9) Gunnlaugsson, T.; Leonard, J. P.; Sénéchal, K.; Harte, A. J. *J. Am. Chem. Soc.* **2003**, *125*, 12062−12063.

(10) Charbonnière, L. J.; Ziessel, R.; Montalti, M.; Prodi, L.; Zaccheroni, N.; Boehme, C.; Wipff, G. *J. Am. Chem. Soc.* **2002**, *124*, 7779−7788.

(11) Harte, A. J.; Jensen, P.; Plush, S. E.; Kruger, P. E.; Gunnlaugsson, T. *Inorg. Chem.* **2006**, *45*, 9465−9474.

(12) Montalti, M.; Prodi, L.; Zaccheroni, N.; Charbonnière, L.; Douce, L.; Ziessel, R. *J. Am. Chem. Soc.* **2001**, *123*, 12694−12695.

(13) Yamada, T.; Shinoda, S.; Tsukube, H. *Chem. Commun.* **2002**, 1218−1219.

(14) Gulgas, C. G.; Reineke, T. M. *Inorg. Chem.* **2008**, *47*, 1548−1559.

(15) Mahajan, R. K.; Kaur, I.; Kaur, R.; Uchida, S.; Onimaru, A.; Shinoda, S.; Tsukube, H. *Chem. Commun.* **2003**, 2238−2239.

(16) Tan, C. L.; Wang, Q. M. *Inorg. Chem.* **2011**, *50*, 2953−2956.

(17) Wang, Q. M.; Tan, C. L. *Anal. Chim. Acta* **2011**, *708*, 111−115.

(18) Ai, K. L.; Zhang, B. H.; Lu, L. H. *Angew. Chem., Int. Ed.* **2009**, *48*, 304−308.

(19) Li, H. R.; Cheng, W. J.; Wang, Y.; Liu, B. Y.; Zhang, W. J.; Zhang, H. J. *Chem.—Eur. J.* **2010**, *16*, 2125−2130.

(20) Yan, B. *RSC Adv.* **2012**, *2*, 9304−9324.

(21) Wang, Q. M.; Tan, C. L.; Chen, H. Y.; Tamiaki, H. *J. Phys. Chem. C* **2010**, *114*, 13879−13883.

(22) Zheng, Y. H.; Tan, C. L.; Wang, Q. M.; Zhang, C. C. *Solid State Sci.* **2011**, *13*, 1687−1691.

(23) Sawicki, M.; Lecerclé, D.; Grillon, G.; Gall, B. L.; Sérandour, A.-L.; Poncy, J.-L.; Bailly, T.; Burgada, R.; Lecouvey, M.; Challeix, V.; Leydier, A.; Pellet-Rostaing, S.; Ansoborlo, E.; Taran, F. *Eur. J. Med. Chem.* **2008**, *43*, 2768−2777.

(24) Zhao, H. J.; Bagwe, R. P.; Tan, W. H. *Adv. Mater.* **2004**, *16*, 173−176.

(25) Yu, Q. Y.; Hui, J. F.; Wang, P. P.; Xu, B.; Zhuang, J.; Wang, X. *Nanoscale* **2012**, *4*, 7114−7120.

(26) Franville, A.-C.; Zambon, D.; Mahiou, R. *Chem. Mater.* **2000**, *12*, 428−435.

(27) Lin, N. N.; Li, H. R.; Wang, Y. G.; Feng, Y.; Qin, D. S.; Gan, Q. Y.; Chen, S. D. *Eur. J. Inorg. Chem.* **2008**, 4781−4785.

(28) Amendola, V.; Bergamaschi, G.; Boiocchi, M.; Fabbrizzi, L.; Mosca, L. *J. Am. Chem. Soc.* **2013**, *135*, 6345−6355.

(29) Amendola, V.; Esteban-Gómez, D.; Fabbrizzi, L.; Licchelli, M. *Acc. Chem. Res.* **2006**, *39*, 343−353.

(30) Jose, D. A.; Kumar, D. K.; Ganguly, B.; Das, A. *Org. Lett.* **2004**, *6*, 3445−3448.

(31) Lima, L. M. P.; Lecointre, A.; Morfin, J.-F.; Blas, D. A; Visvikis, D.; Charbonnière, L. J.; Platas-Iglesias, C.; Tripier, R. *Inorg. Chem.* **2011**, *50*, 12508−12521.

(32) Tripier, R.; Platas-Iglesias, C.; Boos, A.; Morfin, J.-F.; Charbonnière, L. J. *Eur. J. Inorg. Chem.* **2010**, 2735−2745.

(33) Parker, D.; Senanayake, P. K.; Williams, J. A. *J. Chem. Soc., Perkin Trans. 2* **1998**, 2129−2140.

(34) Parker, D.; Senanayake, P. K.; Williams, J. A. *Chem. Commun.* **1997**, 1777−1778.

(35) We would lose very small amounts of powder materials during the recycle experiments. In addition, small quantities of F^- could directly coordinate with Ln^{3+} ions.

(36) Goncalves, M. C.; Bermudez, V. D.; Ferreira, R. A. S.; Carlos, L. D.; Ostrovskii, D. J.; Rocha, J. *Chem. Mater.* **2004**, *16*, 2530−2543.